Lawrence Berkeley Laboratory
UNIVERSITY OF CALIFORNIA

EARTH SCIENCES DIVISION

Transient Diffusion of Radionuclides from a Cylindrical
Waste Solid into Fractured Porous Rock

J. Ahn, P.L. Chambré, and T.H. Pigford

September 1990

DISTRIBUTION OF THIS DOCUMENT IS UNLIMITED

Transient Diffusion of Radionuclides
from a Cylindrical Waste Solid
into Fractured Porous Rock

J. Ahn

Department of Nuclear Engineering
University of Tokyo
Tokyo, Japan

P. L. Chambré and T. H. Pigford

Department of Nuclear Engineering
University of California

and

Earth Sciences Division
Lawrence Berkeley Laboratory
University of California
Berkeley, California 94720

September 1990

MASTER

The authors invite comments and would appreciate
being notified of any errors in the report.

T. H. Pigford
Department of Nuclear Engineering
University of California
Berkeley, CA 94720

CONTENTS

Abstract

Numerical illustrations for transient mass transfer from an infinitely long cylinder intersected by a planar fracture are shown based on Chambré's exact analytical solutions. The concentration at the cylinder surface is maintained at the solubility. In the fracture contaminant diffuses in the radial direction. In the rock matrix three-dimensional diffusion is assumed in the cylindrical coordiante. No advection is assumed. Radioactive decay and sorption equilibrium are included. Comparison between the cylinder model and the previous plane model is given. Radioactive decay enhances the mass transfer from the cylinder. Even though the fracture is assumed to be a faster diffusion path than the rock matrix, the larger waste surface exposed to the matrix and the greater assumed matrix sorption result in greater release rate to the matrix than to the fracture. The cylinder model gives more conservative results than the plane model with respect to the mass transfer from the source and the far-field transport for the diffusion-dominant field.

iv

1 Introduction and Summary

This paper presents the numerical results of an analytical study for mass transfer and transport of radionuclides released from a cylindrical waste solid into water-saturated fractured porous rock. The purposes of this study are (1) to predict the diffusive mass flux from a cylindrical waste solid into a planar fracture and the surrounding rock matrix for the low-flow conditions wherein near-field mass transfer is expected to be controlled by molecular diffusion [1] and (2) to investigate the effects of cylindrical geometry and of multidimensional matrix diffusion including diffusion in the directions parallel to the fracture plane.

Previous analytical studies [2]-[6] of the advective transport of dissolved contaminants through fractured rock have emphasized the effect of molecular diffusion in the rock matrix in affecting the space-time-dependent concentration of the contaminant as it moves along the fracture. Matrix diffusion only in the direction normal to the fracture surface was assumed (Figure 1(a)). Such studies illustrate the far-field transport features of fractured media. To predict the time-dependent mass transfer from a long waste cylinder surrounded by porous rock and intersected by a fracture, the present study includes diffusion from the waste-solid surface directly into porous rock, as well as the more realistic geometry shown in Figure 1(b).

In the following are presented the derivation of an analytical solution for the time-dependent mass transfer from the cylinder for low-flow conditions and computer-code implementation and numerical results. The problem was first proposed and solved analytically by Chambré.

Numerical results are shown for (1) the diffusive mass fluxes from the cylindrical waste solid into the fracture and into the rock matrix, (2) the diffusive mass flux across the rock/fracture interface, and (3) the instantaneous concentration isopleths in the fracture and in the rock matrix.

For the diffusive mass flux from the cylinder, effects of radioactive decay and presence of the fracture are investigated. For shorter-lived nuclides the flux reaches steady state faster and the steady-state flux for the shorter-lived nuclide is greater than the long-lived species. In very early times, the decay effect on release rate is negligible.

Assuming that a dissolving solid is always present, assuming negligible advective transport, and assuming that the fracture has a greater diffusion coefficient and less sorption retardation than the rock matrix, the concentration in the fracture is always greater than in the rock matrix at the same distance from the surface of the dissolving solid. Contaminant diffuses into the rock matrix across the rock/fracture interface, as well as from the waste solid. Consequently, the mass flux from the cylinder into the rock matrix near the fracture is smaller than the flux from the cylinder into the rock matrix in the region far away from the fracture. The effect of the fracture is limited at early time to a very shallow region in the rock matrix. At later times, this effect is negligible so that one can assume that the flux from the cylinder to the rock matrix is independent of the distance from the fracture.

Even though the fracture is assumed to be a faster diffusion path than the rock matrix, the larger waste surface exposed to the matrix and the greater assumed matrix sorption result in greater release rate to the matrix than to the fracture. In this case, we can neglect presence of the fracture, and can apply the analyses for a cylinder surrounded completely by porous rock [4].

Comparison of the present cylindrical model with previous planar models, wherein contaminant was assumed to be released only into the fracture and diffusion in the rock matrix was assumed to be one-dimensional perpendicular to the fracture plane, shows that the cylindrical model is more conservative than the planar models with respect to the mass transfer from the source into the fracture and with respect to the far-field transport, provided that diffusion is dominant in the fracture.

2 Assumptions and Mathematical Formulation

We consider a cylindrical waste solid of infinite length and constant radius $\hat{a}$ [m], intersected by a planar fracture (Figure 1). To be conservative, we assume that no waste container is present. An infinitely long cylinder is a good approximation for a long cylinder with negligible end effects. A constant concentration $\hat{N}^*$ [kg/m^3] of low-solubility dissolved species is prescribed in the water at the waste surface. The contaminant undergoes molecular diffusion both in the fracture and in the rock matrix. The porosities of fracture and
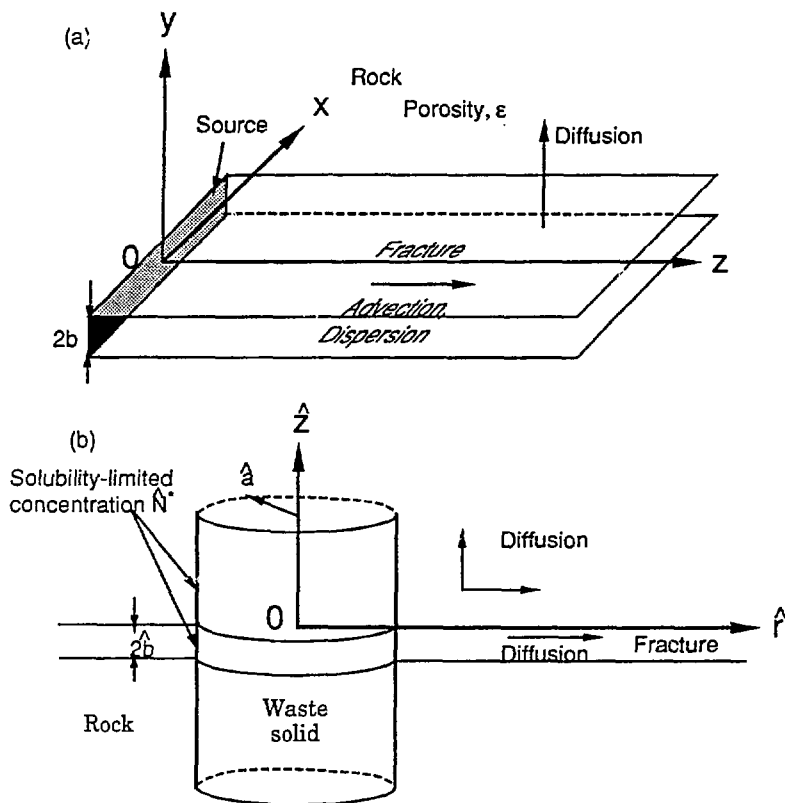
Figure 1: (a) Geometry and physical processes considered in the model with a single, planar, infinite fractures. (b) Cylindrical geometry with three dimensional diffusion in rock matrix and two dimensional diffusion in fracture. Azimuthal symmetry is assumed.

rock are ε_1 and ε_2. Pores are saturated with stationary water. If $\varepsilon_1 < 1$, the fracture is filled with porous sediment. The fracture width, $2\hat{b}$ [m], is assumed to be much smaller than other dimensions such as the cylinder radius, so we assume complete mixing and uniform concentration across the fracture width.

The concentrations in the fracture and in the rock matrix are described in two- and three-dimensional cylindrical coordinate systems, respectively. Different local sorption equilibrium constants are assumed for the fracture and for the rock matrix. Radioactive decay is included, but decay precursors are neglected. Assuming azimuthal symmetry, the governing equations for the space-time-dependent concentrations in the fracture and in the rock matrix are written as:

$$\hat{K}_1 \frac{\partial \hat{N}_1}{\partial \hat{t}} = \frac{\hat{D}_1}{\hat{r}} \frac{\partial}{\partial \hat{r}} \left(\hat{r} \frac{\partial \hat{N}_1}{\partial \hat{r}} \right) - \hat{\lambda} \hat{K}_1 \hat{N}_1 - \frac{\hat{q}(\hat{r}, \hat{t})}{\hat{b}}, \ \hat{r} > \hat{a}, \ \hat{t} > 0, \tag{1}$$

$$\hat{K}_2 \frac{\partial \hat{N}_2}{\partial \hat{t}} = \frac{\hat{D}_2}{\hat{r}} \frac{\partial}{\partial \hat{r}} \left(\hat{r} \frac{\partial \hat{N}_2}{\partial \hat{r}} \right) + \hat{D}_2 \frac{\partial^2 \hat{N}_2}{\partial \hat{z}^2} - \hat{\lambda} \hat{K}_2 \hat{N}_2, \ \hat{z} > 0, \ \hat{r} > \hat{a}, \ \hat{t} > 0, \tag{2}$$

where

$$\hat{q}(\hat{r}, \hat{t}) = - \varepsilon_2 \hat{D}_2 \frac{\partial \hat{N}_2}{\partial \hat{z}} \bigg|_{\hat{z}=0}, \quad \hat{r} > \hat{a}, \ \hat{t} > 0, \tag{3}$$

$\hat{N}_i$: contaminant concentration in water in region i [kg/m^3],

$\hat{D}_i$: diffusion coefficient of the nuclide in region i [m^2/yr],

$\hat{q}$: diffusive flux from the fracture to rock matrix at the interface between rock and fracture [kg/m^2·yr].

$\hat{K}_i$: retardation factor for region i, dimensionless, defined as

$$\hat{K}_i = 1 + \frac{1 - \varepsilon_i}{\varepsilon_i} \hat{K}_{d_i}, \tag{4}$$

λ : radioactive decay constant [yr^{-1}],

ε_i : porosity of region i, dimensionless,

$\hat{r}$: radial distance from the center of the waste cylinder [m],

$\hat{z}$: distance from the interface between fracture and rock [m],

$\hat{t}$: time [yr], and

$\hat{K}_{d_i}$: sorption distribution coefficients in region i, concentration in solid phase divided by concentration in water phase, dimensionless.

Subscripts 1 and 2 refer to fracture and rock, respectively. The hat symbol indicates the quantities with physical dimensions; later we introduce non-dimensionalization. From the assumptions, we can set the side conditions as follows:

$$\hat{N}_1(\hat{r}, 0) = 0, \qquad \hat{r} > \hat{a}, \tag{5}$$

$$\hat{N}_2(\hat{r}, \hat{z}, 0) = 0, \quad \hat{r} > \hat{a}, \ \hat{z} > 0, \tag{6}$$

$$\hat{N}_1(\hat{a}, \hat{t}) = \hat{N}^*, \qquad \hat{t} > 0, \tag{7}$$

$$\hat{N}_1(\infty, t) = 0, \qquad \hat{t} > 0, \tag{8}$$

$$\hat{N}_2(\hat{a}, \hat{z}, \hat{t}) = \hat{N}^*, \quad \hat{z} > 0, \ \hat{t} > 0, \tag{9}$$

$$\hat{N}_2(\infty, \hat{z}, \hat{t}) = 0, \quad \hat{z} > 0, \ \hat{t} > 0, \tag{10}$$

$$\hat{N}_2(\hat{r}, 0, \hat{t}) = \hat{N}_1(\hat{r}, \hat{t}), \quad \hat{r} > \hat{a}, \ \hat{t} > 0, \tag{11}$$

$$\frac{\partial \hat{N}_2}{\partial \hat{z}} \bigg|_{\hat{z} \to \infty} = 0, \quad \hat{r} > a, \ \hat{t} > 0. \tag{12}$$

(3) and (11) provide the coupling of the governing equations.

To simplify further mathematical manipulations, we introduce the following nondimensionalization:

$$r \equiv \frac{\hat{r}}{\hat{a}}, \quad z \equiv \frac{\hat{z}}{\hat{a}}, \quad t \equiv \frac{\hat{D}_2 \hat{t}}{\hat{K}_2 \hat{a}^2} \tag{13}$$

$$\Delta \equiv \frac{\hat{D}_1 \hat{K}_2}{\hat{D}_2 \hat{K}_1}, \quad b \equiv \frac{\hat{b} \hat{K}_1}{\varepsilon_2 \hat{a} \hat{K}_2}, \quad \lambda \equiv \frac{\hat{a}^2 \hat{\lambda} \hat{K}_2}{\hat{D}_2} \tag{14}$$

and

$$N_1(r,t) \equiv \frac{\hat{N}_1(\hat{r},\hat{t})}{\hat{N}^*}, \quad N_2(r,z,t) \equiv \frac{\hat{N}_2(\hat{r},\hat{z},\hat{t})}{\hat{N}^*}, \quad q \equiv \frac{\hat{a}}{\varepsilon_2 \hat{D}_2 \hat{N}^*} \hat{q} \tag{15}$$

The variable t is the Fourier number, which measures the time of the diffusion process. λ is the Thiele modulus. Then, the system of equations (1) to (3) and (5) to (12) can be rewritten as:

$$\frac{\partial N_1}{\partial t} = \frac{\Delta}{r} \frac{\partial}{\partial r} \left(r \frac{\partial N_1}{\partial r} \right) - \lambda N_1 - \frac{q}{b}, \quad r > 1, \quad t > 0, \tag{16}$$

$$\frac{\partial N_2}{\partial t} = \frac{1}{r} \frac{\partial}{\partial r} \left(r \frac{\partial N_2}{\partial r} \right) \frac{\partial^2 N_2}{\partial z^2} - \lambda N_2, \quad r > 1, \quad z > 0, \quad t > 0, \tag{17}$$

where

$$q(r,t) = - \left. \frac{\partial N_2}{\partial z} \right|_{z=0}, \quad r > 1, \quad t > 0, \tag{18}$$

subject to From the assumptions, we can set the side conditions as follows:

$$N_1(r,0) = 0, \quad r > 1, \tag{19}$$

$$N_2(r,z,0) = 0, \quad r > 1, \quad z > 0, \tag{20}$$

$$N_1(1,t) = 1, \quad t > 0, \tag{21}$$

$$N_1(\infty,t) = 0, \quad t > 0, \tag{22}$$

$$N_2(1,z,t) = 1, \quad z > 0, \quad t > 0, \tag{23}$$

$$N_2(\infty,z,t) = 0, \quad z > 0, \quad t > 0, \tag{24}$$

$$N_2(r,0,t) = N_1(r,t), \quad r > 1, \quad t > 0, \tag{25}$$

$$\left. \frac{\partial N_2}{\partial z} \right|_{z \to \infty} = 0, \quad r > a, \; t > 0. \tag{26}$$

We will solve the problem (16)–(26). Since one of our concerns here is mass transfer from the waste solid, we derive the following auxiliary functions:

$$\hat{j}_1(\hat{a},\hat{t}) \equiv -\varepsilon_1 \hat{D}_1 \left. \frac{\partial \hat{N}_1}{\partial \hat{r}} \right|_{\hat{r}=\hat{a}} = \frac{\varepsilon_1 \hat{D}_1 \hat{N}^*}{\hat{a}} j_1(t), \tag{27}$$

and

$$\hat{j}_2(\hat{a},\hat{z},\hat{t}) \equiv -\varepsilon_2 \hat{D}_2 \left. \frac{\partial \hat{N}_2}{\partial \hat{r}} \right|_{\hat{r}=\hat{a}} = \frac{\varepsilon_2 \hat{D}_2 \hat{N}^*}{\hat{a}} j_2(z,t), \tag{28}$$

where

$$j_1(t) \equiv - \left. \frac{\partial N_1}{\partial r} \right|_{r=1}, \quad t > 0, \tag{29}$$

and

$$j_2(z,t) \equiv - \left. \frac{\partial N_2}{\partial r} \right|_{r=1}, \quad z > 0, \quad t > 0. \tag{30}$$

(29) and (30) are the dimensionless diffusive fluxes at the waste surface to the fracture and to the porous rock, respectively. In the following sections analytical forms are obtained and numerical evaluations are shown for (18), (29), and (30) as well as for the concentrations $N_1(r,t)$ and $N_2(r,z,t)$.

3 Derivation of Analytical Solutions

The outline of the solution method is the following: First, apply a Weber transform[7] with respect to r and Laplace transform with respect to t for (16) to (18). Second, solve the second-order ordinary differential equation resulting from (17) and obtain the double-transformed $q(z,t)$. Third, substitute the transformed q into the algebraic equation resulting from (16) and solve the resultant equation. Finally make the inverse transforms twice to obtain the solutions. Important steps to the solution are discussed below.

3.1 Application of Integral Transforms

The Weber transform of a function $f(r)$ for the domain $r > 1$ is defined as:

$$\bar{f}(s) \equiv \int_1^\infty f(r)\Phi(r,s)r\,dr, \quad s > 0, \tag{31}$$

where s is a Weber variable, real, and

$$\Phi(r,s) \equiv J_0(rs)Y_0(s) - Y_0(rs)J_0(s), \tag{32}$$

The overbar symbol stands for a Weber-transform of $f(r)$. With the following formula (see Appendix for derivation):

$$\int_1^\infty \frac{1}{r}\frac{\partial}{\partial r}\left(r\frac{\partial f}{\partial r}\right)\Phi(r,s)r\,dr = -\frac{2}{\pi}f(1) - s^2\bar{f}(s), \quad s > 0, \tag{33}$$

(16) and (17) can be transformed as

$$\frac{d\bar{N}_1}{dt} + \mu_1^2\bar{N}_1 + \frac{\bar{q}}{b} + \frac{2}{\pi}\Delta = 0, \quad s > 0, \ t > 0, \tag{34}$$

$$\frac{\partial\bar{N}_2}{\partial t} + \mu_2^2\bar{N}_2 - \frac{\partial^2\bar{N}_2}{\partial z^2} + \frac{2}{\pi} = 0, \quad s > 0, \ z > 0, \ t > 0, \tag{35}$$

where

$$\mu_1^2 = s^2\Delta + \lambda, \quad \mu_2^2 = s^2 + \lambda, \tag{36}$$

and the boundary conditions (21) and (23) have been used. Next, we apply a Laplace transform on (34) and (35), obtaining

$$(\mu_1^2 + p)\tilde{\bar{N}}_1 + \frac{\tilde{\bar{q}}}{b} + \frac{2\Delta}{\pi p} = 0, \quad s > 0, \tag{37}$$

$$\frac{d^2\tilde{\bar{N}}_2}{dz^2} - (\mu_2^2 + p)\tilde{\bar{N}}_2 - \frac{2}{\pi p} = 0, \quad s > 0, \ z > 0, \tag{38}$$

where p is a Laplace variable, complex, and the tilde, $\tilde{\ }$, denotes the Laplace transformed variable. We will solve (38) subject to the boundary conditions:

$$\tilde{\bar{N}}_2(s,0,p) = \tilde{\bar{N}}_1(s,p), \quad s > 0, \tag{39}$$

$$\left.\frac{d\tilde{\bar{N}}_2}{dz}\right|_{z\to\infty} = 0, \quad s > 0. \tag{40}$$

The solution to (38) satisfying (39), (40) is written as

$$\tilde{\bar{N}}_2(s,z,p) = \left\{\tilde{\bar{N}}_1(s,p) + \frac{2}{\pi p(p+\mu_2^2)}\right\}e^{-z\sqrt{\mu_2^2+p}} - \frac{2}{\pi p(p+\mu_2^2)}, \quad s \geq 0, \ z \geq 0. \tag{41}$$

5

To obtain $\tilde{\bar{N}}_1(s,p)$, we need the expression for $\bar{q}(s,p)$. Differentiating (41) with respect to z and setting z to be zero in the resultant expression, we obtain:

$$\bar{\bar{q}} = \sqrt{\mu_2^2 + p} \left\{ \tilde{\bar{N}}_1(s,p) + \frac{2}{\pi p (p + \mu_2^2)} \right\} \tag{42}$$

Substitution of (42) into (37) yields

$$\tilde{\bar{N}}_1(s,p) = -\frac{2}{\pi p} \left\{ \frac{\Delta}{\tilde{g}(p)} + \frac{1}{b\tilde{g}(p)\sqrt{\mu_2^2 + p}} \right\}, \ s \geq 0, \tag{43}$$

where

$$\tilde{g}(p) = p + \mu_1^2 + \frac{1}{b}\sqrt{\mu_2^2 + p}. \tag{44}$$

Finally, substituting (44) into (41) yields:

$$\tilde{\bar{N}}_2(s,z,p) = \frac{2}{\pi p} \left\{ -\frac{\Delta}{\tilde{g}(p)} - \frac{1}{b\tilde{g}(p)\sqrt{\mu_2^2 + p}} + \frac{1}{\mu_2^2 + p} \right\} e^{-s\sqrt{\mu_2^2 + p}} - \frac{2}{\pi p (\mu_2^2 + p)}, \ s \geq 0, \ z \geq 0. \tag{45}$$

3.2 Inversion of Integral Transforms

We first make inverse Laplace transforms of (43) and (45). Considering that

$$\tilde{g}(p - \mu_2^2) = (\sqrt{p} + \alpha)(\sqrt{p} + \beta), \tag{46}$$

where

$$\alpha \equiv \frac{1 - \Gamma}{2b}, \quad \beta \equiv \frac{1 + \Gamma}{2b}, \quad \Gamma = \sqrt{1 - 4b^2(\Delta - 1)s^2}, \tag{47}$$

the reciprocal of $\tilde{g}$ in (43) and (45) can be reduced to

$$\frac{1}{\tilde{g}(p - \mu_2^2)} = \frac{1}{\beta - \alpha} \left\{ \frac{1}{\sqrt{p} + \alpha} - \frac{1}{\sqrt{p} + \beta} \right\}. \tag{48}$$

Using (48) and the following inversion formulae [8]:

$$\mathcal{L}^{-1} \left[\frac{1}{p} \bar{f}(p) \right] = \int_0^t f(\tau) d\tau, \tag{49}$$

$$\mathcal{L}^{-1} \left[\frac{e^{-k\sqrt{p}}}{\sqrt{p} + a} \right] = \frac{1}{\sqrt{\pi t}} e^{-\frac{k^2}{4t}} - ae^{ak}e^{a^2 t}\text{erfc}\left(a\sqrt{t} + \frac{k}{2\sqrt{t}} \right), \ k \geq 0, \tag{50}$$

$$\mathcal{L}^{-1} \left[\frac{e^{-k\sqrt{p}}}{\sqrt{p}(\sqrt{p} + a)} \right] = e^{ak}e^{a^2 t}\text{erfc}\left(a\sqrt{t} + \frac{k}{2\sqrt{t}} \right), \ k \geq 0, \tag{51}$$

$$\mathcal{L}^{-1} \left[\frac{e^{-k\sqrt{p}}}{p} \right] = \text{erfc}\left(\frac{k}{2\sqrt{t}} \right), \ k \geq 0, \tag{52}$$

the Weber- and Laplace-transformed solutions (43) and (45) can be inverted to:

$$\bar{N}_1(s,t) = -\frac{2}{\pi} \frac{1}{\beta - \alpha} \left[\left(\beta\Delta - \frac{1}{b} \right) F(\beta;0,t) - \left(\alpha\Delta - \frac{1}{b} \right) F(\alpha;0,t) \right], \ s \geq 0, \ t \geq 0, \tag{53}$$

$$\bar{N}_2 = -\frac{2}{\pi} \int_0^t e^{-\mu_2^2 \tau} \text{erf}\left(\frac{z}{2\sqrt{\tau}} \right) d\tau - \frac{2}{\pi} \frac{1}{\beta - \alpha} \left[\left(\beta\Delta - \frac{1}{b} \right) F(\beta;z,t) - \left(\alpha\Delta - \frac{1}{b} \right) F(\alpha;z,t) \right],$$

6

$$s \geq 0, \ z \geq 0, \ t \geq 0, \tag{54}$$

where

$$F(x; z, t) = e^{x^2} \int_0^t e^{(z^2 - \mu_2^2)\tau} \text{erfc}\left(x\sqrt{\tau} + \frac{z}{2\sqrt{\tau}}\right) d\tau. \tag{55}$$

The integral $F(x; z, t)$ converges uniformly in s over $\{s \geq 0\}$ for $t \geq 0$ and $z \geq 0$ to

$$
\begin{aligned}
F(x; z, t) &= \frac{1}{x^2 - \mu_2^2}\left\{ \exp\left(-\mu_2^2 t - \frac{z^2}{4t}\right) H\left(x\sqrt{t} + \frac{z}{2\sqrt{t}}\right) + \frac{x - \mu_2}{2\mu_2} e^{-\mu_2 z}\text{erfc}\left(\frac{z}{2\sqrt{t}} - \mu_2\sqrt{t}\right) \right. \\
&\left. - \frac{x + \mu_2}{2\mu_2} e^{\mu_2 z}\text{erfc}\left(\frac{z}{2\sqrt{t}} + \mu_2\sqrt{t}\right) \right\}, \ t \geq 0, \ z \geq 0, \ s \geq 0, \tag{56}
\end{aligned}
$$

where

$$H(x) = e^{x^2}\text{erfc}(x), \ x \text{ complex}. \tag{57}$$

The first integral in the right hand side of (54) can be obtained by setting $x = 0$ in (56). Then, we obtain the Weber-transformed solutions as:

$$\bar{N}_1(s, t) = -\bar{W}_0(s) - \bar{W}_1(s; 0, t) - \bar{W}_2(s; 0, t) - \bar{W}_4(s; 0, t), \ s \geq 0, \ t \geq 0, \tag{58}$$

$$\bar{N}_2(s, z, t) = -\bar{W}_0(s) - \bar{W}_1(s; z, t) - \bar{W}_2(s; z, t) + \bar{W}_3(s; z, t) - \bar{W}_4(s; z, t), \ s \geq 0, \ z \geq 0, \ t \geq 0, \tag{59}$$

where

$$\bar{W}_0(s) = \frac{2}{\pi}\frac{1}{\mu_2^2}, \tag{60}$$

$$\bar{W}_1(s; z, t) = \frac{1}{\pi}\frac{(\Delta - 1)\lambda}{\mu_2^2\left(\mu_1^2 - \frac{\mu_2}{4}\right)}e^{z\mu_2}\text{erfc}\left(\frac{z}{2\sqrt{t}} + \mu_2\sqrt{t}\right), \tag{61}$$

$$\bar{W}_2(s; z, t) = \frac{1}{\pi}\frac{(\Delta - 1)\lambda}{\mu_2^2\left(\mu_1^2 + \frac{\mu_2}{4}\right)}e^{-z\mu_2}\text{erfc}\left(\frac{z}{2\sqrt{t}} - \mu_2\sqrt{t}\right), \tag{62}$$

$$\bar{W}_3(s; z, t) = \frac{2}{\pi}\frac{1}{\mu_2^2}e^{-\mu_2^2 t}\text{erf}\left(\frac{z}{2\sqrt{t}}\right), \tag{63}$$

and

$$\bar{W}_4(s; z, t) = \frac{2}{\pi}\frac{e^{-\frac{z^2}{4t} - \mu_2^2 t}}{\beta - \alpha}\left\{\frac{\beta\Delta - \frac{1}{b}}{\beta^2 - \mu_2^2}H\left(\beta\sqrt{t} + \frac{z}{2\sqrt{t}}\right) - \frac{\alpha\Delta - \frac{1}{b}}{\alpha^2 - \mu_2^2}H\left(\alpha\sqrt{t} + \frac{z}{2\sqrt{t}}\right)\right\}. \tag{64}$$

Because of the uniform convergence in (56) with respect to s, we can make inverse Weber transforms on (58) and (59) without any restriction on s, obtaining

$$N_1(r, t) = \frac{K_0(\sqrt{\lambda}r)}{K_0(\sqrt{\lambda})} - \{I_1(r, 0, t) + I_2(r, 0, t) + I_4(r, 0, t)\}, \ r \geq 1, \ t \geq 0, \tag{65}$$

$$N_2(r, z, t) = \frac{K_0(\sqrt{\lambda}r)}{K_0(\sqrt{\lambda})} - \{I_1(r, z, t) + I_2(r, z, t) - I_3(r, z, t) + I_4(r, z, t)\}, \ r \geq 1, \ z \geq 0, \ t \geq 0, \tag{66}$$

where

$$I_i(r, z, t) = \int_0^\infty \bar{W}_i(s; z, t)\frac{\Phi(r, s)sds}{[M_0(s)]^2}, \ i = 1, 2, 3, 4, \tag{67}$$

$$M_0(s) = \sqrt{[J_0(s)]^2 + [Y_0(s)]^2}, \tag{68}$$

and $K_0(x)$ modified Bessel function of the zeroth order, $J_0(x)$ and $Y_0(x)$ Bessel functions of the zeroth order, and $\Phi(r, s)$ is defined by (32). The first term in the right hand side of (65) and (66) is obtained by the inverse transform of $\bar{W}_0(s)$ (see Appendix for derivation).

(65) and (66) are the final solutions for the problem (16) to (26). The diffusive fluxes from the waste solid to the fracture and to the rock matrix can be calculated as follows:

$$j_1(t) = \sqrt{\lambda} \frac{K_1(\sqrt{\lambda})}{K_0(\sqrt{\lambda})} - \frac{2}{\pi} \{I_1'(0,t) + I_2'(0,t) + I_4'(0,t)\}, \; t > 0, \tag{69}$$

$$j_2(z,t) = \sqrt{\lambda} \frac{K_1(\sqrt{\lambda})}{K_0(\sqrt{\lambda})} - \frac{2}{\pi} \{I_1'(z,t) + I_2'(z,t) - I_3'(z,t) + I_4'(0,t)\}, \; z \geq 0, \; t > 0, \tag{70}$$

where

$$I_i'(z,t) = \int_0^\infty \bar{W}_i(s;z,t) \frac{sds}{[M_0(s)]^2}, \; i = 1,2,3,4, \tag{71}$$

and the identity [9]:

$$\left. \frac{\partial \Phi(r,s)}{\partial r} \right|_{r=1} = -s\{J_1(s)Y_0(s) - J_0(s)Y_1(s)\} = -\frac{2}{\pi} \tag{72}$$

is used in the course of the derivation.

By differentiating (59) with respect to z and setting z to be zero, we obtain the diffusive mass flux from the fracture to the rock matrix at the interface as:

$$q(r,t) = -I_5''(r,t) + I_6''(r,t), \tag{73}$$

where

$$I_i''(r,t) = \int_0^\infty \bar{W}_i(s;t) \frac{\Phi(r,s)sds}{[M_0(s)]^2}, \; i = 5,6, \tag{74}$$

$$\bar{W}_5(s;t) = \frac{2}{\pi}(\Delta - 1)\lambda \frac{-\frac{1}{b} + \frac{\mu_1^2}{\mu_2}\mathrm{erf}(\mu_2\sqrt{t})}{\mu_1^4 - \frac{\mu_2^2}{b^2}}, \tag{75}$$

$$\bar{W}_6(s;t) = \frac{2}{\pi} \frac{e^{-\mu_1^2 t}}{\beta - \alpha} \left\{ \frac{\beta(\beta\Delta - \frac{1}{b})}{\beta^2 - \mu_2^2} H\left(\beta\sqrt{t}\right) - \frac{\alpha(\alpha\Delta - \frac{1}{b})}{\alpha^2 - \mu_2^2} H\left(\alpha\sqrt{t}\right) \right\}. \tag{76}$$

4 Mathematical Preparation for Numerical Evaluation

4.1 Classification with

We must consider three cases, $\Delta > 1$, $\Delta = 1$, and $\Delta < 1$, separately. By definition of Δ, (14), $\Delta > 1$ means that diffusion is faster in the fracture than in the rock matrix, which is the most likely case. The case $\Delta < 1$ could happen if the fracture is filled with highly sorbing material such as clay. In the case of $\Delta = 1$, the waste cylinder is surrounded entirely by porous rock. The solution to $N_1(r,t)$, (65), then becomes identical to that to $N_2(r,z,t)$, (66). By setting Δ to be unity, we have:

$$\bar{W}_1(s;z,t) = \bar{W}_2(s;z,t) = 0, \; z \geq 0, \; t \geq 0, \; s \geq 0,$$

and $\alpha = 0$, $\beta = \frac{1}{b}$. Therefore,

$$\bar{W}_4(s;z,t) = -\frac{2}{\pi} \frac{1}{\mu_2^2} e^{-\mu_2^2 t} \mathrm{erfc}\left(\frac{z}{2\sqrt{t}}\right),$$

Then, (65) and (66) both reduce to

$$N_1(r,t) = N_2(r,t) = \frac{K_0(\sqrt{\lambda}r)}{K_0(\sqrt{\lambda})} + \frac{2}{\pi} \int_0^\infty \frac{e^{-\mu_2^2 t}}{\mu_2^2} \frac{\Phi(r,s)sds}{[M_0(s)]^2}, \tag{77}$$

8

Notice that (77) is independent of z. For a stable nuclide ($\lambda = 0$), the first term in the right hand side of (77) becomes unity, and the solution (77) becomes identical to the solution for temperature in a region internally bounded by a circular cylinder with a constant temperature at the boundary, obtained by *Carslaw and Jaeger* [10].

For safety assessment of waste disposal, $\Delta > 1$ is likely and conservative, and is so assumed below. In the rest of this section we consider mathematical preparation for numerical evaluation of $N_2(r, z, t)$. j_1, j_2, and q can be treated in a similar way.

4.2   Evaluation of $I_4(r; z; t)$

Assuming $\Delta > 1$ results in evaluation of complementary error functions of a complex argument in $\bar{W}_4(s; z, t)$, (64). From (47) α and β become complex for s in

$$s > s_o \equiv \frac{1}{2b\sqrt{\Delta - 1}}. \tag{78}$$

Therefore, we must divide $I_4(r, z, t)$ into two parts:

$$I_4(r, z, t) = I_{41}(r, z, t) + I_{42}(r, z, t), \tag{79}$$

where

$$I_{41}(r, z, t) = \int_0^{s_o} \bar{W}_4(s; z, t) \frac{\Phi(r, s) s \, ds}{[M_0(s)]^2}, \tag{80}$$

$$I_{42}(r, z, t) = \int_{s_o}^{\infty} \bar{W}_4(s; z, t) \frac{\Phi(r, s) s \, ds}{[M_0(s)]^2}, \tag{81}$$

$$\bar{W}_4(s; z, t) = \{w(\beta; z, t) - w(\alpha; z, t)\} \frac{2}{\pi} \exp\left(-\frac{z^2}{4t} - \lambda t\right) \tag{82}$$

and

$$w(x; z, t) = \frac{e^{-s^2 t}}{\beta - \alpha} \frac{x \Delta - \frac{1}{b}}{x^2 - \mu_2^2} H\left(x\sqrt{t} + \frac{z}{2\sqrt{t}}\right), \quad x = \alpha, \beta. \tag{83}$$

4.2.1 $I_{41}(r, z, t)$

By variable transform from s to Γ, defined as

$$s^2 = (1 - \Gamma^2) s_o^2, \tag{84}$$

the integration interval is changed to $0 \leq \Gamma \leq 1$, and $I_{41}(r, z, t)$ can be written as

$$I_{41}(r, z, t) = \frac{1}{\pi} \exp\left(-\frac{z^2}{4t} - \lambda t\right) \{I_{41}^+(r, z, t) - I_{41}^-(r, z, t)\}, \tag{85}$$

where

$$I_{41}^{\pm}(r, z, t) = \int_0^1 e^{-(1-\Gamma^2) s_o^2 t} w_{\pm}(\Gamma; z, t) \frac{\Phi\left(r, s_o\sqrt{1 - \Gamma^2}\right)}{\left[M_0(s_o\sqrt{1 - \Gamma^2})\right]^2} d\Gamma, \tag{86}$$

$$w_{\pm}(\Gamma; z, t) = \frac{\Delta\Gamma \pm (\Delta - 2)}{\{\Delta\Gamma \pm (\Delta - 2)\}(1 \pm \Gamma) - \lambda/s_o^2} H\left(\frac{\sqrt{t}}{2b}(1 \pm \Gamma) + \frac{z}{2\sqrt{t}}\right). \tag{87}$$

Assuming $\lambda \neq 0$, one may notice that either w_+ or w_- has a singularity inside $0 \leq \Gamma \leq 1$, depending on the values of Δ, b, and λ. If $1 < \Delta \leq 2 + \lambda/s_o^2$, then $w_+(\Gamma; z, t)$ becomes singular at $\Gamma = \Gamma_s = \left\{1 - \Delta + \sqrt{1 + \lambda\Delta/s_o^2}\right\}/\Delta$. If $\Delta > 2 + \lambda/s_o^2$, then $w_-(\Gamma; z, t)$ becomes singular at $\Gamma = \Gamma_s =$

$\left\{ \Delta - 1 - \sqrt{1 + \lambda\Delta/s_o^2} \right\}/\Delta$. These singular points are never the end-point of the integration interval, and so $I_{41}^{\pm}(r,z,t)$ can be considered as the Hilbert transform:

$$I_{41}^{\pm}(r,z,t) = \int_0^1 \frac{f(\Gamma)}{\Gamma - \Gamma_s} d\Gamma, \ 0 < \Gamma_s < 1, \tag{88}$$

where $f(\Gamma)$ can be obtained from (86), (87). The integral is interpreted as a Cauchy principal value. The subroutine D01AQF from the NAG library [11] is suitable for this integration. The subroutine employs a modified Clenshaw-Curtis integration scheme [12] and a global acceptance criterion for error estimation [13]. The same type of singularity is found also in $I_1(r,z,t)$.

If $\lambda = 0$, $w_-(\Gamma; z,t)$ has an end-point singularity at $\Gamma = 1$, while $w_+(\Gamma; z,t)$ has no singularity point inside the interval. This singularity can be removed by the variable transformation from Γ to ξ by

$$\Gamma = 1 - e^{-\xi}. \tag{89}$$

Then, I_{41}^- reduces to

$$I_{41}^-(r,z,t) = \int_0^1 e^{-s_o^2 t A} H\left(\frac{\sqrt{t}}{2b} e^{-\xi} + \frac{z}{2\sqrt{t}}\right) \frac{\Phi\left(r, s_o\sqrt{A}\right)}{\left[M_0(s_o\sqrt{A})\right]^2} d\xi, \tag{90}$$

where $A \equiv 2e^{-\xi} - e^{-2\xi}$. As ξ tends to infinity, A tends to zero, and the H function tends to $H(z/2\sqrt{t})$. If A approaches zero, $Y_0(s_o\sqrt{A})$ in Φ and M_0 tends to $-\infty$. To avoid this difficulty, let us consider the following polynomial approximation [14]:

$$Y_0(x) = \frac{2}{\pi} \ln\left(\frac{x}{2}\right) J_0(x) + a_0 + a_1 \left(\frac{x}{3}\right)^2 + a_2 \left(\frac{x}{3}\right)^4 + \cdots + + a_6 \left(\frac{x}{3}\right)^{12} + \epsilon, \ 0 < x \le 3, \ |\epsilon| < 1.4 \times 10^{-8}, \tag{91}$$

where $a_0 = 0.36746691$, $a_1 = 0.60559366$, $a_2 = -0.74350384$, $a_3 = 0.25300117$, $a_4 = -0.04261214$, $a_5 = 0.00427916$, $a_6 = -0.00024846$.

Substituting $s_o\sqrt{A}$ into x in (91), we may approximate $Y_0(s_o\sqrt{A})$, for large ξ, by

$$Y_0(s_o\sqrt{A}) \approx \frac{1}{\pi}\left(\ln\frac{s_o^2}{2} - \xi\right) + a_0, \ \ J_0(s_o\sqrt{A}) \approx 1. \tag{92}$$

Then, $\Phi(r, s_o\sqrt{A})$ can be approximated, for large ξ, by

$$\Phi(r, s_o\sqrt{A}) \approx \frac{1}{\pi} \ln\left(\frac{1}{r}\right), \tag{93}$$

and $\left[M_0(s_o\sqrt{A})\right]^2$ becomes proportional to $(\xi^2 + \text{const})$ for large ξ. Thus, in the interval $[\xi_c, \infty)$, where ξ_c is determined so that the approximation (92) holds, (90) can be calculated as [15]

$$H\left(\frac{z}{2\sqrt{t}}\right) \frac{1}{\pi} \ln\frac{1}{r} \int_{\xi_c}^{\infty} \left[1 + \left\{\frac{1}{\pi}\left(\ln\frac{s_o^2}{2} - \xi\right) + a_o\right\}^2\right]^{-1} d\xi$$
$$= \frac{1}{\pi} \ln\frac{1}{r} H\left(\frac{z}{2\sqrt{t}}\right) \left\{\frac{\pi}{2} - \tan^{-1}\left(\frac{\xi_c - \pi a_0 - \ln(s_o^2/2)}{\pi}\right)\right\}. \tag{94}$$

In the rest of the interval, i.e., $[0, \xi_c]$, (90) is evaluated numerically by Gaussian quadratures without difficulty. The same type of singularity occurs also in $I_3(r,z,t)$.

4.2.2 $I_{42}(r, z, t)$

In the interval $s > s_o$, α and β become complex. For a complex argument, the error function can be evaluated by the following formula [16]:

$$\text{erf}(x + yi) = R(x, y) + iI(x, y), \tag{95}$$

where

$$R(x, y) = \text{erf}(x) + \frac{e^{-x^2}}{2\pi x}(1 - \cos 2xy) + \frac{2}{\pi}e^{-x^2}\sum_{n=1}^{\infty}\frac{e^{-\frac{1}{4}n^2}}{n^2 + 4x^2}f_n(x, y), \tag{96}$$

$$I(x, y) = \frac{e^{-x^2}}{2\pi x}\sin 2xy + \frac{2}{\pi}e^{-x^2}\sum_{n=1}^{\infty}\frac{e^{-\frac{1}{4}n^2}}{n^2 + 4x^2}g_n(x, y), \tag{97}$$

$$f_n(x, y) = 2x - 2x\cosh(ny)\cos(2xy) + n \cdot \sinh(ny)\sin(2xy), \tag{98}$$

and

$$g_n(x, y) = 2x\cosh(ny)\sin(2xy) + n \cdot \sinh(ny)\cos(2xy), \tag{99}$$

With (95)-(99) and the variable transformation:

$$\gamma = \sqrt{\frac{s^2}{s_o^2} - 1}, \tag{100}$$

$I_{42}(r, z, t)$ can be rewritten as follows:

$$I_{42}(r, z, t) = \frac{2}{\pi}\exp\left(-\frac{z^2}{4t} - (\lambda + s_o^2)t\right)\left\{\phi\left(\frac{b}{\sqrt{t}}\Omega\right)I_{421}(r, z, t) - I_{422}(r, z, t)\right\}, \tag{101}$$

where

$$I_{421}(r, z, t) = \int_0^{\infty}\frac{e^{-\Delta s_o^2 t\gamma^2}}{D(\gamma)}\{A(\gamma)\sin(\Omega\gamma) - B(\gamma)\cos(\Omega\gamma)\}\frac{\Phi\left(r, s_o\sqrt{1 + \gamma^2}\right)}{\left[M_0\left(s_o\sqrt{1 + \gamma^2}\right)\right]^2}d\gamma, \tag{102}$$

$$I_{422}(r, z, t) = \int_0^{\infty}\frac{e^{-s_o^2 t\gamma^2}}{D(\gamma)}S(\gamma)\frac{\Phi\left(r, s_o\sqrt{1 + \gamma^2}\right)}{\left[M_0\left(s_o\sqrt{1 + \gamma^2}\right)\right]^2}d\gamma, \tag{103}$$

$$\phi(x) = H(x) - \frac{1}{2\pi x} - \frac{4x}{\pi}\sum_{n=1}^{\infty}\frac{e^{-\frac{1}{4}n^2}}{n^2 + 4x^2}, \tag{104}$$

$$A(\gamma) = \sigma(\gamma) - (\Delta - 2)\frac{\lambda}{s_o^2}, \quad B(\gamma) = \gamma\left\{\sigma(\gamma) + \frac{\lambda\Delta}{s_o^2}\right\}, \tag{105}$$

$$D(\gamma) = (\gamma^2 + 1)\sigma(\gamma) + \frac{2\lambda}{s_o^2}\left(\Delta\gamma^2 - \Delta + 2\right) + \frac{\lambda^2}{s_o^4}, \tag{106}$$

$$S(\gamma) = \frac{B(\gamma)}{2\pi x}\exp\left(-\frac{t\gamma^2}{4b^2}\right) + \frac{1}{\pi}\sum_{n=1}^{\infty}\frac{2xB(\gamma) + nA(\gamma)}{n^2 + 4x^2}\exp\left\{-\frac{1}{4}\left(n - \frac{\sqrt{t}}{b}\gamma\right)^2\right\} \tag{107}$$

$$+ \frac{1}{\pi}\sum_{n=1}^{\infty}\frac{2xB(\gamma) - nA(\gamma)}{n^2 + 4x^2}\exp\left\{-\frac{1}{4}\left(n + \frac{\sqrt{t}}{b}\gamma\right)^2\right\},$$

$$\sigma(\gamma) = \Delta^2\gamma^2 + (\Delta - 2)^2, \ \Omega = \frac{t}{2b^2} + \frac{z}{2b}, \ x = \frac{b}{\sqrt{t}}\Omega. \tag{108}$$

The function $\phi(x)$ vanishes quite rapidly for $x > 1$. Therefore, $I_{421}(r, z, t)$ may be evaluated only for $x < 1$.

11

4.3 Evaluation of $I_2(r;z;t)$

By a variable transform,

$$\xi = \sqrt{p^2 + \lambda}, \tag{109}$$

$I_2(r,z,t)$ can be rewritten as

$$I_2(r,z,t) = \frac{(\Delta - 1)\lambda}{\pi} \int_{\sqrt{\lambda}}^{\infty} e^{-z\xi} \mathrm{erfc}\left(\frac{z}{2\sqrt{t}} - \sqrt{t}\xi\right) K(\xi) \Phi\left(r, \sqrt{\xi^2 - \lambda}\right) d\xi, \tag{110}$$

where

$$K(\xi) = \frac{1}{\xi \left\{\Delta \xi^2 + (1 - \Delta)\lambda + \frac{\xi}{t}\right\} \left[M_0\left(\sqrt{\xi^2 - \lambda}\right)\right]^2}. \tag{111}$$

If $\frac{z}{2\sqrt{t}} - \sqrt{\lambda t} > 0$, then the argument of the complementary error function is positive for $\xi \in \{\sqrt{\lambda} < \xi < \frac{z}{2t}\}$. Then, the combination of the exponential and the complementary error functions can be evaluated by using the H function defined by (57):

$$e^{-z\xi} \mathrm{erfc}\left(\frac{z}{2\sqrt{t}} - \sqrt{t}\xi\right) = \exp\left(-\frac{z^2}{4t} - \xi^2 t\right) H\left(\frac{z}{2\sqrt{t}} - \sqrt{t}\xi\right) \tag{112}$$

For $\xi \in \{\xi > \frac{z}{2t}\}$, the above combination can be calculated as follows:

$$e^{-z\xi} \mathrm{erfc}\left(\frac{z}{2\sqrt{t}} - \sqrt{t}\xi\right) = e^{-z\xi} \left\{2 - \mathrm{erfc}\left(\sqrt{t}\xi - \frac{z}{2\sqrt{t}}\right)\right\} = 2e^{-z\xi} - \exp\left(-\frac{z^2}{4t} - \xi^2 t\right) H\left(\sqrt{t}\xi - \frac{z}{2\sqrt{t}}\right). \tag{113}$$

If $\frac{z}{2\sqrt{t}} - \sqrt{\lambda t} \leq 0$, then the argument of the complementary error function is always non-positive. (113) can be used for the entire integration interval.

In summary, $I_2(r,z,t)$ can be evaluated with the following formula:

$$I_2(r,z,t) = \frac{1}{\pi}(\Delta - 1)\lambda \left\{ \begin{array}{ll} \left[e^{-\frac{z^2}{4t}} I_{21} + \left\{I_{22}\left(\frac{z}{2\sqrt{t}}\right) - e^{-\frac{z^2}{4t}} I_{23}\left(\frac{z}{2\sqrt{t}}\right)\right\}\right], & \text{for } \frac{z}{2\sqrt{t}} - \sqrt{\lambda t} > 0, \\ \left[I_{22}(\sqrt{\lambda}) - e^{-\frac{z^2}{4t}} I_{23}(\sqrt{\lambda})\right] & \text{for } \frac{z}{2\sqrt{t}} - \sqrt{\lambda t} \leq 0, \end{array} \right. \tag{114}$$

where

$$I_{21} \equiv \int_{\sqrt{\lambda}}^{\frac{z}{2\sqrt{t}}} f_{21}(\xi) d\xi, \text{ where } f_{21}(\xi) = e^{-\xi^2 t} H\left(\frac{z}{2\sqrt{t}} - \sqrt{t}\xi\right) K(\xi) \Phi\left(r, \sqrt{\xi^2 - \lambda}\right), \tag{115}$$

$$I_{22}(k) \equiv \int_k^{\infty} f_{22}(\xi) d\xi, \text{ where } f_{22}(\xi) = 2e^{-z\xi} K(\xi) \Phi\left(r, \sqrt{\xi^2 - \lambda}\right), \tag{116}$$

$$I_{23}(k) \equiv \int_k^{\infty} f_{23}(\xi) d\xi, \text{ where } f_{23}(\xi) = e^{-\xi^2 t} H\left(\sqrt{t}\xi - \frac{z}{2\sqrt{t}}\right) K(\xi) \Phi\left(r, \sqrt{\xi^2 - \lambda}\right), \tag{117}$$

Due to the $\exp(-\xi^2 t)$ term, the interval for I_{23} may be replaced by a finite one.

4.4 Oscillation of Integrands

Due to the presence of $\Phi(r,s)$, all integrands in $N_1(r,t)$, $N_2(r,z,t)$, and $q(r,t)$ oscillate. How rapidly they oscillate depends on how large r is. For the cases of $I_3(r,z,t)$ and $I_4(r,z,t)$, the integrands vanish quite rapidly because of the term, $\exp(-\mu_2^2 t)$, so that the integration interval can be considered to be finite. If the computer underflow limit is e^{-U}, then the integration may be performed in the interval of $0 \leq s \leq \sqrt{\frac{U}{t} - \lambda}$. On the other hand, the integrands of $I_1(r,z,t)$ and $I_2(r,z,t)$ vanish much more slowly, so one may have to integrate over hundreds of cycles of oscillation to evaluate the integrals with enough accuracy. For such slowly convergent integrands, the ϵ^1-transformation for slowly convergent series and integrals [17] is employed.

12

For the evaluation of the flux, $j_2(z,t)$, we may consider the case without the function, $\Phi\left(r, \sqrt{\xi^2 - \lambda}\right)$, in the above formulation. Here we do not have oscillation, so numerical evaluation is easier. However, without oscillation, the evaluation of (116) for $z = 0$ or very small z needs special care. In $j_2(z,t)$ the integral corresponding to (116) is written as

$$I_{22}(k) \equiv \int_k^\infty f_{22}(\xi)d\xi, \text{ where } f_{22}(\xi) = 2e^{-z\xi}K(\xi). \tag{118}$$

$f_{22}(x)$ decreases very slowly if z is very small or zero. We can evaluate (118) by speed-up of convergence with the help of B-transform [13].

5 Numerical Evaluations

Computer programs are implemented for $N_2(r,z,t)$, $j_2(z,t)$ and $q(r,t)$. $N_1(r,t)$ and $j_1(t)$ can be calculated by setting $z = 0$ in the input data for the programs for $N_2(r,z,t)$, and $j_2(z,t)$, respectively. Programs are written in FORTRAN 77.

5.1 Input Data Formats

For the flux, $j_2(z,t)$, input data can be either with or without dimensions. Table 1 shows the format. For the flux, $q(r,t)$, data for z or $\hat{z}$ in Table 1 are replaced by those for r or $\hat{r}$.

For the concentration $N_2(r,z,t)$, one can obtain results as a function of r, z, or t, or as an isopleth. One must use nondimensionalized values as input data.

5.2 Input Data

We assume that the waste solid comes from the spent fuel of a pressurized-water reactor. The radius of the cylinder is $\hat{a} = 25$ cm. Fracture width $2\hat{b}$ is 1 cm. Surrounding rock has porosity $\varepsilon_2 = 0.01$, whereas the fracture has no filling material ($\varepsilon_1 = 1$). The diffusion coefficient is the same for both fracture and rock, and is conservatively chosen as that for a liquid continuum (500 cm^2/yr). Sorption on fracture walls is neglected ($\hat{K}_1 = 1$). Sorption in the rock matrix is assumed to retard the matrix diffusion process by the factor $\hat{K}_2 = 500$. Three actinides and a stable nuclide are compared in the numerical results: ^{234}U ($\hat{\lambda} = 2.806 \times 10^{-6}$ yr^{-1}), ^{241}Am ($\hat{\lambda} = 1.513 \times 10^{-5}$ y^{-1}), and 239Pu ($\hat{\lambda} = 2.841 \times 10^{-5}$ yr^{-1}). With these values, non-dimensionalized parameters can be calculated as:

$$b = 0.004, \ \Delta = 500, \ t = 1.6 \times 10^{-3} \ \hat{t} \ [\text{yr}]$$

and

$$\lambda = 1.754 \times 10^{-3} \text{ for } {}^{234}\text{U}, \ \lambda = 0.9456 \text{ for } {}^{241}\text{Am}, \ \lambda = 1.7755 \times 10^{-2} \text{ for } {}^{239}\text{Pu}.$$

5.3 Features of Diffusive Mass Transfer in Cylindrical Geometry

Figure 2 gives an overall idea of how the contaminant is transfered from a cylinder and is transported in the fractured porous rock. Shown there are instantaneous concentration isopleths, mass flux from the cylinder to rock, mass flux to the fracture, and flux across the rock/fracture interface for ^{239}Pu at Fourier number $t = 1$, which corresponds to 625 yr for the parameter values shown above. The concentration in rock is larger near the cylinder and near the fracture. The concentration isopleth shows that the influence of the fracture on the concentration in the rock matrix becomes negligible beyond five radii from the rock/fracture interface. The mass flux from the cylinder into the fracture is calculated to be about two orders of magnitude greater than that into the rock matrix because of the assumed hundred-fold greater porosity in the fracture. The mass flux into the rock matrix becomes smaller in the vicinity of the fracture because contaminant diffusing

Table 1: Input data format for flux j_2 calculation

(1) For values with dimensions

Line	Parameter	Explanation
1	'inp'	input 'phy' to indicate that the following data have dimensions
2	$\hat{K}_1, \hat{K}_2$	retardation factors
3	$\hat{D}_1, \hat{D}_2$	diffusion coefficients
4	ε_2	porosity of rock
5	$\hat{a}, \hat{b}$	cylinder radius and half-width of fracture
6	nxl, 'xax'*	
7 ⋮ 6 + nxl	$\hat{\lambda}$	decay constants
nxl+7	nt, 'tax'*	
nxl+8 ⋮ nxl+nt+7	$\hat{t}$	time
nxl+nt+8	nz, 'zax'*	
nxl+nt+9 ⋮ nxl+nt+nz+8	$\hat{z}$	distance from the fracture/rock interface

(2) For nondimensionalized values

Line	Parameter	Explanation
1	'inp'	input 'non' to indicate that the values are nondimensionalized.
2	Δ, b	
3	nxl, 'xax'*	
4 ⋮ 3 + nxl	λ	Thiele moduli
nxl+4	nt, 'tax'*	
nxl+5 ⋮ nxl+nt+4	t	Fourier numbers
nxl+nt+5	nz, 'zax'*	
nxl+nt+6 ⋮ nxl+nt+nz+5	z	normalized distance from the fracture/rock interface

* For these character data, 'var' or 'par' can be input. If 'var' is input, that variable is considered to be principal and others are parameters.

14

Table 2: Input data format for concentration calculation

(1) For an isopleth:

Line		Explanation
1	'inp'	input 'contour' to indicate that the following data are for an isopleth.
2	$\Delta,\ b,\ \lambda$	
3	t	
4	nr	
5 ⋮ nr+4	r	normalized distance from the cylinder center
nr+5	nz	
nr+6 ⋮ nr+nz+5	z	normalized distance from the rock/fracture interface.
nr+nz+6	nline	number of contour lines. Contour lines are drawn for 10^{-1} to $10^{-1-nline}$.

(2) For one variable cases:

Line	Parameter	Explanation
1	'inp'	input 'one-dim' to indicate that the following data are for one-variable case.
2	$\Delta,b,\ \lambda$	
3	nr, 'rax'‡	
4 ⋮ nr+3	r	
nr+4	nz, 'zax'‡	
nr+5 ⋮ nr+nz+4	z	
nr+nz+5	nt, 'tax'‡	
nr+nz+6 ⋮ nr+nz+nt+5	t	

‡One of these three must be input as 'var', 'par', or 'fix'. The variable for which 'var' is input is considered as the horizontal axis. If 'par' is input, the variable is a parameter.
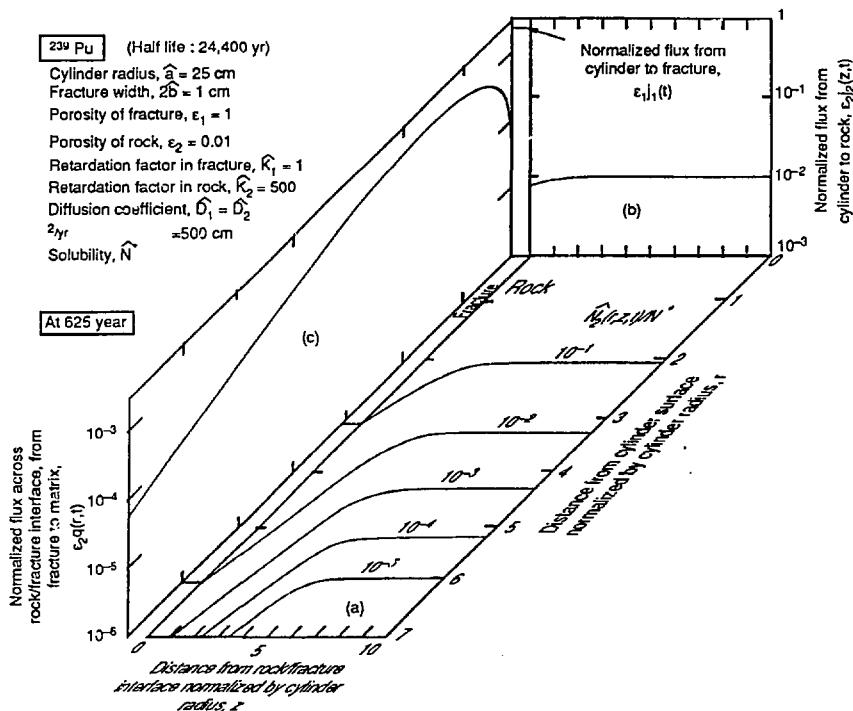
239 Pu (Half life : 24,400 yr)

Cylinder radius, $\hat{a}$ = 25 cm
Fracture width, $2\hat{b}$ = 1 cm
Porosity of fracture, ε_1 = 1

Porosity of rock, ε_2 = 0.01
Retardation factor in fracture, $\hat{K}_1$ = 1
Retardation factor in rock, $\hat{K}_2$ = 500
Diffusion coefficient, $\hat{D}_1 = \hat{D}_2$
$2_{/yr}$ =500 cm
Solubility, $\hat{N}$

At 625 year

Normalized flux from
cylinder to fracture,
$\varepsilon_1 J_1(t)$

10^{-1}

10^{-2}

(b)

10^{-3}

Normalized flux from
cylinder to rock, $\varepsilon_2 j_2(z,t)$

1

(c)

Fracture   Rock

$\hat{N}_2 f(r,z,t)/N$

10^{-1}

10^{-2}

10^{-3}

10^{-4}

10^{-5}

(a)

Distance from cylinder surface
normalized by cylinder radius, r

Normalized flux across
rock/fracture interface, from
fracture to matrix,
$\varepsilon_2 q(r,t)$

10^{-3}

10^{-4}

10^{-5}

10^{-6}

0   5   10

Distance from rock/fracture
interface normalized by cylinder
radius, z

Figure 2: Illustration of nuclide migration at 625 year, or Fourier number 1: (a) isopleths of normalized concnetration in fracture and in rock, (b) normalized flux from waste cylinder to rock, and (c) normalized flux from fracture to rock.
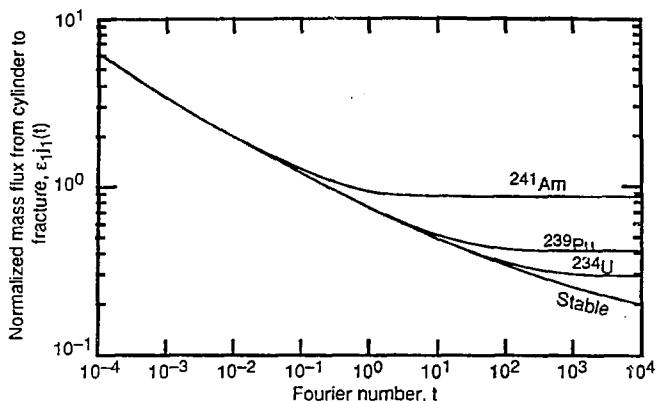
Figure 3: Mass fluxes for three radionuclides and a stable nuclide from the cylinder to the fracture at the cylinder surface as a function of time. Parameters from Figure 2 apply.

from the fracture reduces the concentration difference between the surface of the cylinder and inside the rock matrix.

The mass flux across the interface between rock and fracture is zero at the surface of the cylinder ($r = 1$) because of the boundary conditions at $r = 1$. The concentration difference increases with the distance from the cylinder surface because of the assumed larger retardation factor and smaller porosity in rock matrix, so concentration in the rock matrix decreases faster with distance than in the fracture. Mass flux across the interface starts to decrease after it reaches the maximum because both concentrations in the fracture and in the rock matrix approach zero.

The maximum results from mass transfer from the cylinder directly into the rock matrix and from diffusion parallel to the fracture plane. In the plane model (Figure 1(a)), where matrix diffusion is assumed to be only perpendicular to the fracture plane, the diffusive mass flux at the fracture/rock interface shows the monotonically decreasing profile against the distance from the source. The comparison between the two models is mentioned later.

Figure 3 shows the changes of mass flux from the cylinder to the fracture with Fourier number for three actinides and a stable nuclide. In very early times effect of decay is not apparent. Curves for shorter-half-life nuclides deviate from that to a stable nuclide at an earlier time and reach steady state. For a stable nuclide the mass flux approaches zero as time increases. Because of the loss by radioactive decay during diffusion in the medium, less of the shorter-half-life nuclides will reach a given distance from the surface. Therefore, the steady-state concentration gradient is steeper for shorter-half-life nuclides. Thus, radioactive decay enhances the long-term mass transfer from the cylinder to the rock matrix and to the fracture.

In Figure 4 mass flux of ^{239}Pu from the cylinder to the rock matrix is depicted as a function of Fourier number. The location $z = 0+$ is located at the rock-matrix side of the interface. The curve for $z = 0+$ is, therefore, a hundred-fold less than that for $j_1(t)$, shown in the previous figure. In early times the effect of the fracture on rock-matrix diffusion is limited to the vicinity of the fracture, and there the mass flux is much lower than the mass flux to the rest of the rock matrix. For example, at $t = 10^{-3}$, in $z > 0.1$, the mass flux from the cylinder is virtually uniform, but the difference between the flux in the region $z > 0.1$ and the flux at the fracture-rock interface is large. As time increases, the affected region extends to greater z, and the differences in mass fluxes become small. At $t = 10^2$ and later the mass fluxes are essentially uniform over z.

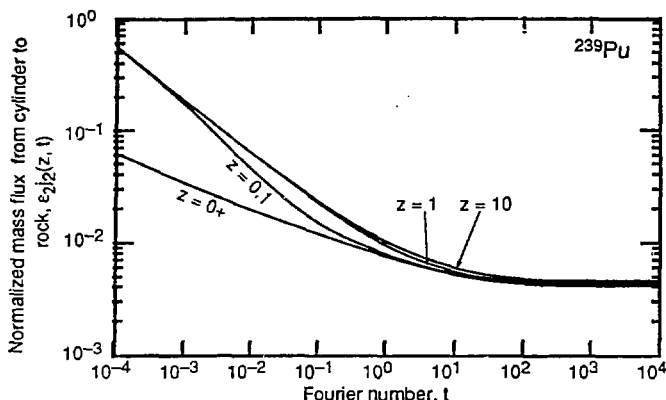Figure 5 illustrates the effect of the Thiele modulus, or radioactive decay, on the mass flux to the fracture.

Figure 4: Normalized mass flux of ^{239}Pu from the cylinder to the rock matrix at the cylinder surface as a function of Fourier number. Four curves depict the effect of diffusion from the fracture to the rock matrix. Parameters from Figure 2 apply.

In early times, for long-half-life nuclides, radioactive decay has no effect. At $t = 10^{-2}$ only ^{90}Sr and ^{3}H have short enough half-lives to affect the mass flux. By $t = 10^2$, mass fluxes of ^{234}U, ^{239}Pu, and ^{241}Am are also affected by radioactive decay. A curve for each Fourier number starts to increase at some value of the Thiele modulus. Curves merge with each other at large Thiele modulus.

Figure 6 shows the profiles of the mass flux of ^{239}Pu at the rock/fracture interface from the fracture to the rock matrix as a function of distance from the waste surface. As seen in Figure 2, there is a maximum along r, which is quite different from what has been observed in planar geometry in the previous study [19]. At $r = 1$, the mass flux is zero because of the boundary conditions (21) and (23). Because diffusion in the rock matrix is slower than in the fracture, the concentration in the fracture is always larger than that in rock matrix if compared at the same distance from the cylinder surface. As r tends to infinity, both concentrations tend to zero. Therefore, there should be a maximum mass flux between $r = 1$ and infinity. The maximum value decreases and the location of the maximum advances with time. Because both concentrations approach steady state, the profile for $t = 10^4$ shows only slight change from $t = 10^2$.

5.4 Validity of the Cylinder Model

As material is released, the cylinder radius will decrease with time, so the boundary conditions (21) and (23) may be valid only within limited time. The waste is in a cylindrical borehole, with water filling the annular space between the waste and rock. Liquid in the annulus will be well mixed by diffusion and convection. If the liquid is saturated at the waste surface, it will be saturated throughout the annulus. Therefore, the saturated concentration at $r = 1$ will maintain.

The finite initial inventory of radionuclides in the waste cylinder requires an upper bound of time for applicability of the present model. For this purpose we consider a cumulative mass release from the cylinder. Cumulative mass releases to the fracture and to the rock matrix are defined as:

$$\hat{M}_1(\hat{t}) = \int_0^{\hat{t}} \hat{j}_1(\hat{\tau})d\hat{\tau} \cdot 2\pi\hat{a} \, 2\hat{b} \, [g], \tag{119}$$
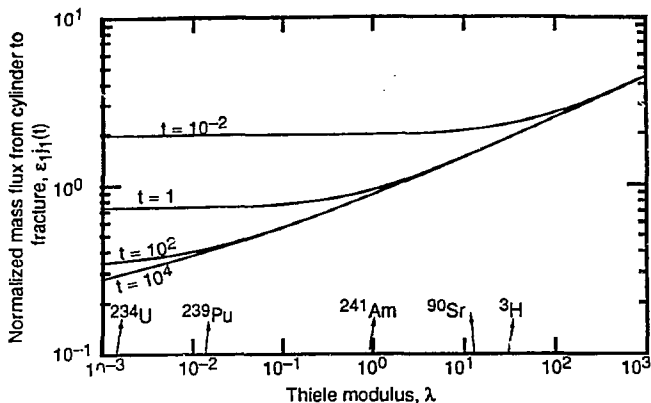
18

Figure 5: mass flux from the cylinder to the fracture as a function of Thiele modulus. Typical radionuclides are indicated at the corresponding Thiele Moduli, which can be calculated by assuming the parameter values applied in Figure 2.
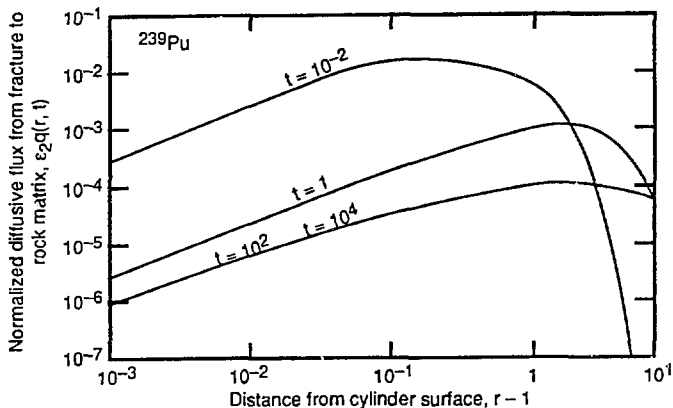

Figure 6: Diffusive flux across the interface between rock and fracture from fracture to rock matrix, as a function of distance from the cylinder surface. The curve for Fourier number of 10,000 is so close to that for 100.

19

and

$$\dot{M}_2(t) = \int_0^{\hat{t}} \int_0^{\frac{\hat{L}}{2}-\hat{b}} \hat{j}_2(\hat{z}, \hat{\tau}) d\hat{z} \ \cdot \ 2 \times 2\pi \hat{a} d\hat{\tau} \ [\text{g}], \tag{120}$$

respectively. By (27), (29), (28), (30) and (13), (119), (120) can be written in terms of Fourier number and non-dimensionalized mass fluxes, $j_1(t)$ and $j_2(z,t)$ as:

$$\dot{M}_1(t) = 4\pi \hat{a}^2 \hat{b} \varepsilon_1 \hat{K}_2 \frac{\hat{D}_1}{\hat{D}_2} \hat{N}^* \int_0^t j_1(\tau) d\tau, \tag{121}$$

and

$$\dot{M}_2(t) = 4\pi \hat{a}^3 \varepsilon_2 \hat{K}_2 \hat{N}^* \int_0^t \int_0^{(\hat{L}-2\hat{b})/2\hat{a}} j_2(z, \tau) dz d\tau, \tag{122}$$

respectively, where t is Fourier number.

From the numerical results shown in Figure 4, the z-dependency of $j_2(z,t)$ is becomes negligible at later times, and the value of $j_2(z,t)$ at the cylinder ends is always the greatest in the surface exposed to the rock matrix. So, instead of calculating the integral with respect to z in (122), we approximate the integral by the value of $j_2(z,t)$ at the cylinder ends multiplied by the length, $\frac{\hat{L}/2-\hat{b}}{\hat{a}}$. Then, (122) can be estimated approximately, but conservatively as follows:

$$\dot{M}_2(t) \le 4\pi \hat{a}^2 \hat{K}_2 \hat{N}^* \varepsilon_2 \left(\frac{\hat{L}}{2} - \hat{b} \right) \int_0^t j_2 \left(\frac{\hat{L}/2 - \hat{b}}{\hat{a}}, \tau \right) d\tau. \tag{123}$$

If the initial inventory of the nuclide of interest in the unit length of the waste cylinder is $\hat{w}^o$ [g/cm], amount of the nuclide in the cylinder $\hat{L}$ is $\hat{L}\hat{w}^o$ [g]. Normalized with this amount, the total cumulative release of the nuclide from the cylinder to the fracture and to the rock matrix is now written as:

$$\dot{M}_{\text{total}}(t) \le R \left\{ \frac{\varepsilon_1 \hat{b} \hat{D}_1}{\hat{L} \hat{D}_2} \int_0^t j_1(\tau) d\tau + \frac{\varepsilon_2}{2} \int_0^t j_2 \left(\frac{\hat{L}/2 - \hat{b}}{\hat{a}}, \tau \right) d\tau \right\}, \tag{124}$$

where

$$R = \frac{4\pi \hat{a}^2 \hat{K}_2 \hat{N}^*}{\hat{w}^o}. \tag{125}$$

The present model is valid until $\dot{M}_{\text{total}}(t)$ becomes unity.

For a spent fuel we assume $\hat{L} = 300$ cm, where $\hat{L}$ is the length of a spent-fuel assembly. In one assembly, there are 2,300 g of ^{239}Pu, 230 g of ^{241}Am, and 88 g of ^{234}U [18]. If the solubility of these three nuclides is assumed to be $\hat{N}^* = 10^{-9}$ g/cm^3, we have:

For ^{239}Pu, $\hat{w}^o = 7.67$ g/cm, $R = 5.12 \times 10^{-4}$
For ^{241}Am, $\hat{w}^o = 0.767$ g/cm, $R = 5.12 \times 10^{-3}$
For ^{234}U, $\hat{w}^o = 0.293$ g/cm, $R = 1.34 \times 10^{-2}$.

In Figure 7 plotted are $\dot{M}_{\text{total}}(t)$ versus Fourier number. These curves do not reach unity even at 10^4 of the Fourier number, which corresponds to 6.25 million years, for ^{239}Pu, ^{241}Am and ^{234}U.

In Figure 8 the amount of radionuclide released into rock matrix is compared with that into the fracture. Instantaneous release rate into the fracture is defined as:

$$\dot{m}_1(t) = 2\hat{b} \cdot 2\pi \hat{a} j_1(t) = 4\pi \hat{a} \hat{D}_2 \hat{N}^* \left(\varepsilon_1 \frac{\hat{b} \hat{D}_1}{\hat{a} \hat{D}_2} \right) j_1(t). \tag{126}$$

Instantaneous release rate into the rock matrix is defined as:

$$\dot{m}_2(t) = 2 \times 2\pi \hat{a} \int_0^{\frac{\hat{L}}{2}-\hat{b}} \hat{j}_2(\hat{z}, t) d\hat{z} = 4\pi \hat{a} \hat{D}_2 \hat{N}^* \varepsilon \int_0^{\frac{\hat{L}}{2a}-\frac{\hat{b}}{a}} j_2(z,t) dz. \tag{127}$$
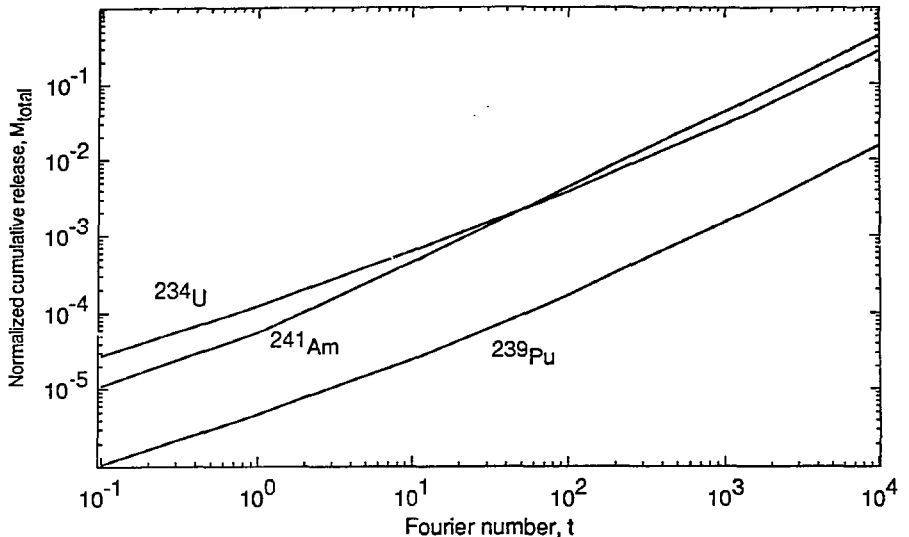
20

Figure 7: Cumulative mass release from the cylinder, normalized by the initial inventory of each species in the cylinder of 3 m high.

In Figure 8 release rates are normalized by the factor $4\pi\hat{a}\hat{D}_2\hat{N}^*$. Even though the mass flux from the waste into the rock matrix is low relative to that into fracture, the larger waste surface exposed to the matrix and the greater assumed matrix sorption result in greater release rate to the matrix than to the fracture. This indicates that for the parameters assumed here, the earlier mass-transfer theory [4] for a waste solid completely surrounded by porous rock can adequately predict release rates in low-flow conditions in fractured rock. If tortuosity significantly reduces the diffusion coefficient in the rock matrix and not in the fracture, mass-transfer directly from the waste to the fracture becomes more important.

5.5 Comparison of the Cylinder Model with the Planar Model

In [19] we studied the one-dimensional advective-dispersive transport in the fracture associated with one-dimensional matrix diffusion in the planar geometry. The contaminant is released only to the fracture. We compare in this section the planar model with the cylinder model. We make the following assumptions for the planar model. The planar source exposed to the fracture is assumed to be the constant-concentration boundary. No advection is assumed in the fracture ($v = 0$).

The models are compared in two ways: (1) mass fluxes from the source, and (2) far-field transport.

For mass transfer from the source, we adopt from [19] the expression for the mass flux from the plane source to the fracture, comparable to (27):

$$\hat{j}_p(\hat{t}) = \frac{\hat{N}^*}{\sqrt{\pi}}\sqrt{\hat{A}\hat{D}\hat{R}_f}\int_0^{\sqrt{\hat{t}/\hat{A}}}\left\{\exp\left(-\frac{\mu^4}{4(\hat{t}-\mu^2\hat{A})} - \hat{\lambda}\hat{t}\right)\left[\left(\hat{\lambda} - \frac{\sqrt{\hat{\lambda}}}{\hat{A}}\right)\right.\right.$$
$$H\left(\frac{\mu^2}{2\sqrt{\hat{\lambda}(\hat{t}-\mu^2\hat{A})}} + \sqrt{\hat{\lambda}(\hat{t}-\mu^2\hat{A})}\right) + \frac{1}{\hat{A}}\frac{2\hat{t}-\mu^2\hat{A}}{(\hat{t}-\mu^2\hat{A})^{3/2}}\right]$$
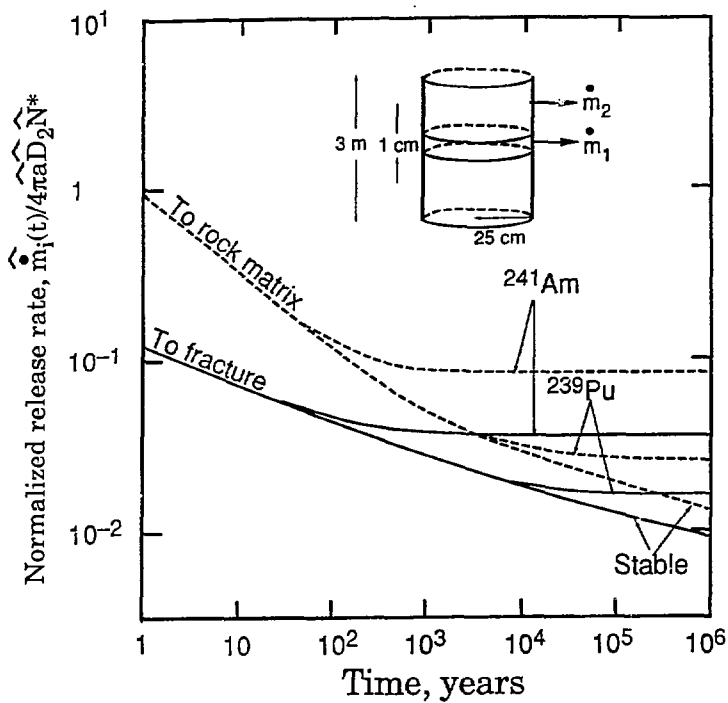
Figure 8: Normalized release rate of nuclides from a 3 m-high waste cylinder. Geologic parameters from Figure 2 apply.

$$+ \left(\hat{\lambda} + \frac{\sqrt{\hat{\lambda}}}{\hat{A}} \right) \exp\left(-\hat{\lambda}\hat{A}\mu^2 - \sqrt{\hat{\lambda}}\mu^2 \right) \text{erfc} \left(\frac{\mu^2}{2\sqrt{\hat{t} - \mu^2 \hat{A}}} - \sqrt{\hat{\lambda}(\hat{t} - \mu^2 \hat{A})} \right) \right\} d\mu, \ \hat{t} > 0, \quad (128)$$

where

$$\hat{A} = \frac{\hat{b}\hat{R}_f}{\epsilon\sqrt{\hat{D}_p \hat{R}_p}}, \quad (129)$$

and

ϵ : porosity of the rock matrix (the fracture is assumed to be completely open in the planar model),

$\hat{R}_f$: retardation factor for the fracture transport,

$\hat{R}_p$: retardation factor for the matrix diffusion,

$\hat{D}$: diffusion coefficient in the fracture, and

$\hat{D}_p$: diffusion coefficient in the rock matrix.

Here the symbol ^ indicates that the quantities have dimensions. The subscript p stands for planar geometry.

For far-field transport, the steady-state solutions are useful. From (65), as t increases, the concentration in the fracture for the cylinder case approaches:

$$N_1^s(r) = \frac{K_0\left(\sqrt{\lambda}r\right)}{K_0\left(\sqrt{\lambda}\right)} - \frac{2}{\pi}(\Delta - 1)\lambda \int_0^\infty \frac{1}{\mu_2^2\left(\mu_1^2 + \frac{\mu_2}{b}\right)} \frac{\Phi(r,p)}{\left[M_0(p)\right]^2} p \, dp, \ r \geq 1. \quad (130)$$

Superscript s stands for steady state. For the planar model, from [19] the steady-state solution for the concentration in the fracture for zero advection and the constant-concentration boundary is available as:

$$\hat{N}^s(\hat{z}) = \hat{N}^* \exp\left\{ -\sqrt{\frac{\hat{\lambda}\hat{R}_f}{\hat{D}} + \frac{\epsilon\sqrt{\hat{D}_p\hat{\lambda}\hat{R}_p}}{\hat{D}\hat{b}}} \, \hat{z} \right\} \quad (131)$$

where $\hat{z}$ is the distance from the plane source.

For the numerical results shown in Figures 9 and 10, the values in Table 3 are assumed.

In Figure 9 the mass flux from the source, normalized by the source-boundary concentration, is plotted against time in years. For the cylinder, the curves are identical to the curves in Figure 3; only the scaling of the axes is changed. In early times both geometries give close results. As time proceeds, the planar model yields smaller mass fluxes, and the difference between the two models at steady state is greater for longer-lived radionuclides.

In cylindrical geometry, the contaminant is dispersed through more volume of the medium as it progresses farther away from the cylinder-source surface. So the mass transfer from the source is greater in cylindrical geometry than in planar geometry. On the other hand, because there is no matrix diffusion parallel to the fracture, the diffusive flux at the interface between fracture and rock becomes larger in the planar model than in the cylinder model, especially in the vicinity of the source surface. More material would be removed from the fracture in the planar model, resulting in greater mass transfer from the source. The numerical results in Figure 9 show that cylindrical geometry increases mass transfer from the source more than does one-dimensional matrix diffusion.

In Figure 10, the normalized concentrations in the fracture at steady state are compared. The horizontal axis represents the distance from the source surface; $\hat{r} - \hat{a}$, in the cylinder case, and $\hat{z}$ in the planar case. In the region near the source, the planar model gives greater concentrations, whereas in the far region the
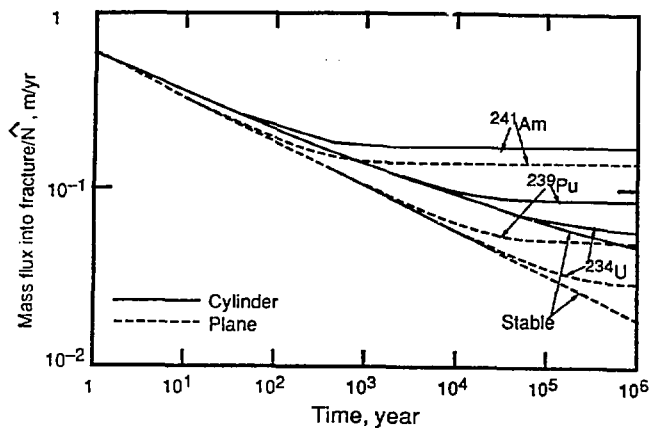
23

Figure 9: Comparison of the diffusive mass flux from the source in the cylinder model with that in the plane model. Parameter values in Table 3 apply.

Table 3: Summary of assumed parameter values

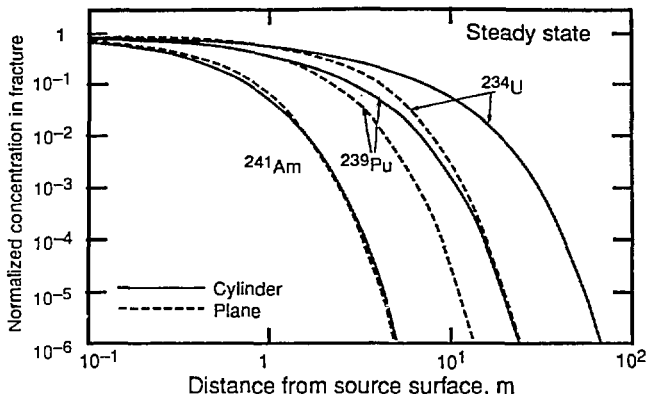|		nomenclature		value
		cylinder	planar	
cylinder radius		$\hat{a}$	—	25 cm
fracture aperture		$\hat{b}$		1 cm
porosity	fracture	ε_1	—	1
	rock	ε_2	ϵ	0.01
water velocity		—	v	0
retardation coefficients	fracture	$\hat{K}_1$	$\hat{R}_f$	1
	rock	$\hat{K}_2$	$\hat{R}_p$	500
diffusion coefficients	fracture	D_1	D	0.05 m^2/yr
	rock	$\hat{D}_2$	$\hat{D}_p$	0.05 m^2/yr

24

Figure 10: Concentration profiles in the fracture, normalized by the source concentration. Parameter values in Table 3 apply.

cylinder model is more conservative. For shorter half-life nuclides such as ^{241}Am, the difference is negligible, but for ^{234}U, the difference is prominent.

Because the contaminant is released into the rock matrix as well as to the fracture in the cylinder model, less contaminant in the fracture can diffuse into the rock matrix than in the planar model. Consequently, for the cylinder more contaminant is transported in the fracture, resulting in greater concentration in the far field. For short-lived nuclides, because radioactive decay is predominant, the effect of parallel matrix diffusion is not apparent.

Thus both for the near-field mass transfer and for the far-field transport, the cylinder model gives conservative results, provided that molecular diffusion is the sole transport mechanism in the medium.

6 Conclusions

Mass fluxes to the fracture and to the rock matrix reach steady state for radioactive contaminants. Shorter half-life nuclides reach steady state earlier. In very early times the effect of radioactive decay is negligible. Radioactive decay enhances mass transfer from the cylindrical waste solid, from the comparison of the magnitudes of the steady-state mass fluxes.

Because of diffusion from fracture to rock, the mass flux from the cylinder to rock matrix is smaller in the region near the fracture than in regions far from the fracture. The effect of the presence of the fracture is limited to a shallow region in the rock matrix in early times. From the numerical result for ^{239}Pu, after a Fourier number of 100 the fracture effect on the mass flux from the cylinder to rock matrix can be neglected, and the mass flux to the rock matrix becomes virtually constant over the waste surface.

The present model is applicable for more than six million years, which is long enough for the purpose of performance assessment study.

Although the mass flux from the waste to the fracture can be as much as hundred-fold larger than that to the rock matrix because of complete openness of the fracture, the total amount of the nuclide released into the rock matrix can become greater than that to the fracture because the waste surface in contact with the rock matrix is much larger than that in contact with the fracture. Under such conditions the model for a cylinder surrounded completely by porous rock matrix is adequate.

25

Three-dimensional diffusion in the rock matrix, as well as the release from the cylinder to the rock matrix and to the fracture, result in quite different features of transport in the fracture, when compared with transport in the planar geometry. The cylinder model is more conservative than the planar model with respect to mass transfer from the source and to far-field transport.

Appendices: On Weber Transforms

A.1 Derivation of (33)

Integrating the left hand side of (33) with respect to r, we obtain:

$$\int_1^\infty \frac{1}{r}\frac{\partial}{\partial r}\left(r\frac{\partial f}{\partial r}\right)\Phi(r,s)rdr = \left[r\frac{\partial f}{\partial r}\Phi(r,s)\right]_1^\infty - \int_1^\infty r\frac{\partial f}{\partial r}\frac{\partial \Phi}{\partial r}dr. \tag{132}$$

For large arguments of $J_0(z)$ and $Y_0(z)$ [20],

$$J_0(z) \approx \sqrt{\frac{2}{\pi z}}\left\{\cos\left(z-\frac{\pi}{4}\right) + O\left(|z|^{-1}\right)e^{|\mathrm{Im}\ z|}\right\}, \tag{133}$$

$$Y_0(z) \approx \sqrt{\frac{2}{\pi z}}\left\{\sin\left(z-\frac{\pi}{4}\right) + O\left(|z|^{-1}\right)e^{|\mathrm{Im}\ z|}\right\}, \tag{134}$$

$$|\arg z| < \pi,\ |z| \to \infty,\ z\ \text{complex}$$

For a real x, these reduce to

$$J_0(x) \approx \sqrt{\frac{2}{\pi x}}\left\{\cos\left(x-\frac{\pi}{4}\right) + O\left(x^{-1}\right)\right\}, \tag{135}$$

$$Y_0(x) \approx \sqrt{\frac{2}{\pi x}}\left\{\sin\left(x-\frac{\pi}{4}\right) + O\left(x^{-1}\right)\right\}, \tag{136}$$

$$x \to \infty.$$

Therefore,

$$\Phi(r,s) \sim O\left(r^{-1/2}\right). \tag{137}$$

We assume that $f(r)$ is Weber-transformable, i.e.. the integral $\int_1^\infty f(r)\sqrt{r}dr$ exists [7], and $f(r)$ is continuous over $r \in [1,\infty)$. Then,

$$f(r) \sim O\left(r^{-1/2-\alpha}\right),\ \ \frac{\partial f}{\partial r} \sim O\left(r^{-3/2-\alpha}\right), \alpha > 0. \tag{138}$$

Because $\Phi(1,s) = 0$, the first term of the right hand side of (132) vanishes. If we integrate the second term in the right hand side of (132) by parts once more, then we obtain:

$$\int_1^\infty r\frac{\partial f}{\partial r}\frac{\partial \Phi}{\partial r}dr = \left[rf(r)\frac{\partial \Phi}{\partial r}\right]_1^\infty - \int_1^\infty f(r)\frac{\partial}{\partial r}\left(r\frac{\partial \Phi}{\partial r}\right)dr. \tag{139}$$

Similarly,

$$\lim_{r\to\infty} rf(r)\frac{\partial \Phi}{\partial r} = 0.$$

At $r = 1$, $\frac{\partial \Phi}{\partial r}$ can be evaluated as follows [21]:

$$\left.\frac{\partial \Phi}{\partial r}\right|_{r=1} = s\left\{-J_1(rs)Y_0(s) + J_0(s)Y_1(rs)\right\}_{r=1} = s\left(-\frac{2}{\pi s}\right) = -\frac{2}{\pi}$$

26

Therefore, the first term in the right hand side of (139) becomes:

$$\left[r f(r) \frac{\partial \Phi}{\partial r} \right]_1^\infty = \frac{2}{\pi} f(r). \tag{140}$$

By differentiating $\Phi(r, s)$ twice with respect to r,

$$\frac{\partial}{\partial r} \left(r \frac{\partial \Phi}{\partial r} \right) = -s^2 \Phi(r, s). \tag{141}$$

From (140) and (141), the result follows.

A.2 Inverse Weber Transform of $W_0(s)$

Consider the following problem:

$$\frac{1}{r} \frac{d}{dr} \left(r \frac{df}{dr} \right) - \lambda f = 0, \quad r > 1, \tag{142}$$

subject to

$$f(1) = 1, \quad f(\infty) = 0. \tag{143}$$

Applying the Weber transform on (142) yields

$$\bar{f}(s) = -\frac{2}{\pi} \frac{1}{s^2 + \lambda}. \tag{144}$$

This implies that the Weber transform of the solution to (142) is (144). The solution to (142) is known as

$$f(r) = \frac{K_0 \left(r \sqrt{\lambda} \right)}{K_0 \left(\sqrt{\lambda} \right)}$$

Then, the inverse Weber transform of (60) is obtained as above.

References

[1] Chambré, P. L., and T. H. Pigford, Predictions of Waste Performance in a Geologic Repository, *Scientific Basis for Nuclear Waste Management VII*, edited by G. L. McVay, New York: Elsevier, 985, 1983,

[2] Neretnieks, I., Diffusion in the Rock Matrix: An important Factor in Radionuclide Retardation?, *J. Geophys. Res.*, 85, 4379, 1980,

[3] Tang, D. H., E. O. Frind, and E. A. Sudicky, Contaminant Transport in Fractured Porous Media: Analytical Solution for a Single Fracture, *Water Resources Res.*, 17, 555, 1981,

[4] Chambré, P. L., T. H. Pigford, A. Fujita, T. Kanki, R. Kobayashi, H. Kung, D. Ting, Y Sato, S. Zavoshy, *Analytical Performance Models for Geologic Repositories*, LBL-14842, 1982,

[5] Ahn, J., P. L. Chambré, and T. H. Pigford, *Radionuclide Migration Through Fractured Rock: Effect of Multiple Fractures and Two Member Decay Chains*, LBL-21121, 1985,

[6] Ahn, J., P. L. Chambré, T. H. Pigford, and W. W.-L. Lee, *Radionuclide Dispersion from Multiple Patch Sources into a Rock Fracture*, LBL-23425, 1986,

[7] Griffith, J. L., On Weber Transforms, *J. and Proc. of the Royal Soc. New South Wales*, LXXXIX, Part 4, 232, 1955,

[8] Abramowitz, M., and I. A. Stegun, *Handbook of Mathematica Functions with Formulas, Graphs, and Mathematical Tables*, 10th ed., Chapter 29, Dover, New York, 1972,

[9] *ibid.*, Identity 9.1.16,

[10] Carslaw, H. S., and J. C. Jaeger, *Conduction of Heat in Solids*, Second ed., 13.5, Oxford Univ. Press, New York, 1959,

[11] *NAG library Mark 10*, Numerical Algorithm Group,

[12] Piessens, R., E. de Doncker-Kapenga, C. W. berhuber, and D. K. Kahaner, *QUADPACK : A Subroutine Package for Automatic Integration*, Springer-Verlag, Berlin Heidelberg, 1983,

[13] Davis, P. J., and P. Rabinowitz, *Methods of Numerical Integration*, Second ed., Academic Press, Orlando, 1984,

[14] Same as [8], Identity 9.4.2,

[15] Gradshteyn, I. S., and I. M. Ryzhik, *Table of Integrals, Series, and Products*, Corrected and Enlarged Ed., Identity 2.141, Academic Press, Orlando, 1980,

[16] Salzer, H. E., Formulas for Calculating the Error Function of a Complex Variable, *Math. Tables Aids Comp.*, 5, 67, 1951,

[17] Shanks, D., Non-Linear Transformations of Divergent and Slowly Convergent Sequences, *J. Math. and Phys.*, 34, 1, 1955,

[18] Waste Isolation Systems Panel, Board on Radioactive Waste Management, National Research Council, *A Study of the Isolation System for Geological Disposal of Radioactive Waste,* National Academy Press, Washington D. C., 1983,

[19] Ahn, J., P. L. Chambré, and T. H. Pigford, *Nuclide Migration through a Planar Fissure with Matrix Diffusion*, LBL-19429, 1985.

[20] Same as [8], Identities 9.2.1 and 9.2.2,

[21] Same as [8], *Identity 9.1.16.*